RSC Advances

ROYAL SOCIETY OF CHEMISTRY

www.rsc.org/advances

Journal Name

ARTICLE

MoO_2 Nanocrystals Interconnected on Mesocellular Carbon Foam as Powerful Catalyst for Vanadium Redox Flow Battery

Received 00th January 20xx,
Accepted 00th January 20xx

DOI: 10.1039/x0xx00000x

www.rsc.org/

Hien Thi Thu Pham[a],‡, Changshin Jo[b],‡, Jinwoo Lee[b],*, and Yongchai Kwon[a],**

To increase performance of vanadium redox flow battery (VRFB), slow reaction of VO^{2+}/VO_2^+ redox couple known as rate determining reaction should be enhanced. For promoting the slow reaction, molybdenum dioxide nanocrystals interconnected on mesocellular carbon foam (MoO_2/MSU-F-C) are suggested as a new catalyst. Initially, optimal amount of MoO_2 embedded on MSU-F-C is determined, while its activity, reversibility and charge-discharge behavior are investigated. Their specific surface area, crystal structure, surface morphology and component analysis are also measured using BET, XRD, TEM, TGA, EELS and XPS. As a result, the MoO_2/MSU-F-C results in high peak current, small peak potential difference and high electron transfer rate constant, confirming that the composite is excellent catalyst for VO^{2+}/VO_2^+ redox reaction. In terms of the multiple charge-discharge tests, VRFB single cell including MoO_2/MSU-F-C induces high voltage and energy efficiencies with high specific capacity and low capacity loss rate. These results are attributed to intercalation of MoO_2 occurred by metal cations like VO^{2+} and VO_2^+ and hydrophilic functional groups existed on surface of MoO_2/MSU-F-C. The intercalated MoO_2 plays an excellent conductor role in promoting fast ionic and electron transfers and reducing overpotential, while the hydrophilic functional groups improve VO^{2+}/VO_2^+ redox reaction by lowering its activation energy.

1 Introduction

As demands for continuous development and exploitation of renewable energies such as solar cell and wind power increase, the deployment of large scale energy storage system (ESS) is getting indispensable. Redox flow batteries (RFBs) have been acknowledged as a viable candidate for the large scale ESS.[1-4] The RFB is electrochemical system that converse and store energy by redox reactions of redox couples and many efforts have been made in opting the best redox couples and RFB system. Among those numerous kinds of RFB, to date, all vanadium redox flow batteries (VRFBs) have attracted much attention due to their various positive characteristics.[3-9] In the VRFB, both electrodes are filled with solutions including four different vanadium ions. In positive electrode, the reservoir is filled with VO^{2+}/VO_2^+ redox couples, while the other reservoir is filled with V^{3+}/V^{2+} in negative electrode. With the use of the same kind of redox couples making up with vanadium ions, additional advantages like low cross contamination of metal cations, low environmental impact and long lifetime are also possible.[10,11]

However, in spite of that, mass production of the VRFB has not been realized yet due to its still low electrochemical activity, followed by low VRFB performance.[12] Since the electrochemical activity and VRFB performance are completed by competition of reactions occurring in both electrodes, it is critical to find out the rate determining one between reactions occurring at the two electrodes and to increase its reaction rate. Regarding the rate determining reaction, it was known that the reaction rate of redox couple (VO^{2+}/VO_2^+) taking place at positive electrode was lower and more complicated than that (V^{2+}/V^{3+}) occurring at negative electrode.[13,14] Previous research results showed that the low VO^{2+}/VO_2^+ reaction rate was mainly attributed to (i) unfavorable surface conditions of

[a] Graduate school of Energy and Environment, Seoul National University of Science and Technology, 232 Gongneung-ro, Nowon-gu, Seoul, 139-743, Republic of Korea.
[b] Department of Chemical Engineering, Pohang University of Science and Technology (POSTECH), 77 Cheongam-ro, Nam-gu, Pohang, Kyungbuk 790-784, Republic of Korea.

‡ HTT Pham and C Jo contributed equally to this work and should be co-first authors
**Corresponding author. Tel: +82 29706805, Fax: +82 29706800, E-mail address: kwony@seoultech.ac.kr
*Corresponding author. Tel: +82 54 2792395, Fax: +82 54 2795528, E-mail address: jinwoo03@postech.ac.kr
Electronic Supplementary Information (ESI) available: [details of any supplementary information available should be included here]. See DOI: 10.1039/x0xx00000x

electrode material and (ii) complicated reaction steps (one electron and two proton transfers).[15]

To overcome such problems, there have been extensive attempts. Of them, graphite felt was selected as a baseline electrode material due to its affordable surface area and good stability in acidic solution.[12] However, hydrophobic property of the graphite felt surface prevented further facilitation of VO^{2+}/VO_2^+ reaction because the VO^{2+}/VO_2^+ redox reaction was prohibited in hydrophobic surface and more activated in hydrophilic surface. To fortify the hydrophilicity and increase reactivity of the VO^{2+}/VO_2^+ reaction, two ideas have been recently considered – (i) oxidation of graphite felt and (ii) utilization of noble metal catalyst.

Oxidized graphite is getting attention because oxygen functional groups facilitating vanadium reaction are more heavily contained in the structure, maintaining unique merits of graphite.[16] Also, noble metals like Pt, Pd and Ir have been used to enhance catalytic activity of the vanadium redox reaction.[4,17-19] But, in case of graphite oxide, reduction issue of electron/ion conductivity should be addressed, while noble metal catalysts are very expensive and sensitive to undesirable hydrogen evolution reaction. As another approach to promote the vanadium redox reaction, adoption of cheap metal oxides such as Mn_3O_4, WO_3 and Nb_2O_5 has been suggested.[20,21] It was also proved that use of the metal oxides induced improvement in VRFB performance although degree of the improvement was not significant.

In this study, to pave the way for enhancing the $VO^{2+/}VO_2^+$ reaction and the VRFB performance, we suggest a new catalyst that is configured as a combinational structure of mesocellular carbon foam (MSU-F-C) and metal oxide nanocrystal (MoO_2). The MSU-F-C consists of large interconnected pores and was opened to all directions. Therefore, ions and electrons can diffuse fast through pores of the MSU-F-C. Also, it includes oxygen functional groups and they play a role in increasing the vanadium redox reaction, while other features of carbon remained unchanged. In detailed explanation, C-O and C=O bonds of the oxygen functional groups are main components to influence the vanadium redox reaction.[5,22] Namely, the carbon-oxygen bonds act as active sites, catalyzing VO^{2+}/VO_2^+ redox reaction. For example, during charge process ($VO^{2+} \rightarrow VO_2^+$), VO^{2+} ions are diffused to electrode and react with hydrogen that is adjacent to C-O bond on the electrode surface. Electron is then transferred from VO^{2+} ions to the electrode along with the C-O-V bond. Oxygen atom released from C-O of surface is bonded with VO^{2+} to form VO^+_2. Finally, VO^+_2 ions are replaced by H^+ ion provided from electrolyte and moves back to the electrolyte. By such mechanism, electron transfer is facilitated from C-O-V bond and VO^{2+} ion is bonded with oxygen atom released from C-O to generate VO^+_2. In discharge process ($VO_2^+ \rightarrow VO^{2+}$), opposite reactions to charge process take place.

Unlike other metal oxide candidates attempted so far, the molybdenum dioxide (MoO_2) nanocrystal has the distorted rutile structure and is famous for its low electrical resistivity, high chemical stability in acidic solution, high volume capacity and high surface acidity. Due to the advantages, catalysts including MoO_2 have been used in the fields of lithium-ion batteries and hydrogen storage. Thus, it is anticipated that use of the MoO_2 may promote the vanadium redox reaction.[23-25]

Taken together, addition of the new catalyst consisting of MSU-F-C and MoO_2 on the graphite felt probably result in positive effect regarding vanadium redox reaction and VRFB performance. Following the employment of MSU-F-C and MoO_2 on graphite felt, its catalytic activity and VRFB performance were investigated to estimate whether the catalyst affected facilitation of VO^{2+}/VO_2^+ redox reaction and enhancement in VRFB performance.

2 Experimental

2.1 Synthesis of catalysts

Synthesis of Mesocellular carbon foam, MSU-F-C, was already reported and we followed the procedure for this study.[26,27] To generate acidic sites on silica template, the MSU-F silica was mixed with $AlCl_3$ in DI water solution (Si/Al weight ratio is 20). After drying, the mixture was heat-treated at 550 °C under air. As a carbon source, 1 g of furfuryl alcohol was impregnated to pores of 1 g of aluminated MSU-F silica with incipient wetness method. After polymerization at 85 °C for 5 h under vacuum, the material was carbonized at 850 °C for 2 h under Ar flow. To remove the aluminated silica, the product was stirred in 5 wt% HF solution for 8 h, followed by washing with DI water.

For the MoO_2 impregnation, 0.1 g of MSU-F-C was dispersed in 20 ml of ethanol. To impregnate molybdenum precursors, different weights (0.05, 0.1, and 0.15g) of phosphomolybdic acid (PMA) hydrates were added to MSU-F-C/ethanol solution. After stirring for 30 min, the mixture was dried at 60 °C and calcined at 500 °C in H_2/N_2 (4wt % H_2) atmosphere for 3 h (1 °C/min).

2.2 Catalytic activity and reversibility measurements

Electrochemical measurements like cyclic voltammetry (CV) were implemented using a computer connected potentiostat (CHI 720D, CH Instrument, USA). The CV was performed to estimate (i) catalytic activity and reaction reversibility of VO^{2+}/VO_2^+ reaction and (ii) electron transfer rate constant. Pt wire was used as a counter electrode and Ag/AgCl (soaked in 3M KCl) was acted as a reference electrode. To build up working electrode, catalytic powder was mixed with isopropanol and 5 wt. % Nafion solution under sonication for 3 min. After mixing, the catalytic ink was dropped on glass carbon disk electrode (GCE) with loading amount of 7 μL. After loading, the working electrode was dried for 1 h at room temperature.[28,29]

As an electrolyte for VRFB tests, 1M $VOSO_4$ + 1M H_2SO_4 mixture was used. Vanadium solution used was prepared by dissolving $VOSO_4$ (Sigma Aldrich, 97%) to H_2SO_4 with stirring and all tests were performed at room temperature. In particular, potential scan rate was used for determining both the rate determining process and the electron transfer rate constant by using Laviron's model. In all the related tests,

potential scan rate of CVs increased from 5 to 50 mV s^{-1} by an increment of 5 mV s^{-1}.

2.3 VRFB single cell fabrication and cyclic tests of charge-discharge sequence

VRFB single cells had the same configuration with previously reported ones.[4-6] As both positive and negative electrodes, a PAN graphite felt (XF30A, Toyobo, Japan) that is 5 mm thick was used. Total active area of the single cell was 4 cm^2 and Nafion 212 was used as membrane. The tanks placed in both negative and positive electrodes were filled with a solution including 1 M $VOSO_4$ + 1M H_2SO_4. The $VOSO_4$ and H_2SO_4 solutions were mixed under vigorous stirring until the blue color of V^{4+} appeared.[6]

To evaluate the effect of catalyst coated on the graphite felt on VRFB performance, catalysts were sprayed onto surface of the graphite felt. The catalyst powder of 10 mg was initially mixed with 750 µL isopropanol and 20 µL Nafion and the ink was sonicated for 3 min and then coated on the graphite felt using airspraying. The VRFB single cell tests consisted of pre-activation step, charging step and discharging step. We used the same procedure to previously reported ones.[4,5]

2.4 Characterization of catalysts

The structure of MoO_2/MSU-F-C and pure MSU-F-C was characterized by scanning electron microscopy (SEM, S-4200 field emission SEM, Hitachi) and transmission electron microscopy (TEM, JEM-1011, Jeol LTD). Electron energy loss spectroscopy (EELS) images were collected by high-resolution TEM (HR-TEM, Jeol EM-2010). Powder X-ray diffraction (XRD) patterns were obtained using a Bruker D8 Advance X-ray diffractometer (Cu Kα radiation). The Nitrogen physisorption was conducted using a Tristar II 3020 instrument at 77 K (Micromeritics Instrument Co.). NETZSCH STA 449C thermobalnce was used for the thermogravimetric analysis (TGA, heating rate: 2 ^oC min^{-1}). To characterize surface states and degree of functional groups, XPS (ESCA LAB250, VG Scientific) analysis was performed. A water contact angle analysis was conducted by contact angle measurement system (Krüss, Model DSA-10, Hamburg, Germany) with 7 µL deionized water. The drop of water was recorded by a web-camera (@info, ALC-M1000).

3 Results and discussion

3.1 Structural characterizations of the corresponding catalysts

The schematic illustration explaining synthesis of MoO_2/MSU-F-C samples is shown in Scheme 1. MSU-F-C was prepared by a hard template method using mesocellular silica foam as a template.[22] Structure of the MSU-F-C consists of (i) cellular pores with diameters of ~30 nm and (ii) small pores additionally generated by removal of silica template. The large and 3-D open pores facilitate access of electrolyte into the carbon surface while high surface area of MSU-F-C provides abundant active sites for high loading of MoO2 particles.[30,31] For MoO_2 catalyst loading, the different weights of molybdenum precursors (phosphomolybdic acid hydrate, PMA) were impregnated inside the pores. The ratio of precursor to MSU-F-C was 0.5:1, 1:1, and 1.5:1, respectively and the catalysts are denoted as MoO_2/MSU-F-C-1, MoO_2/MSU-F-C-2, and MoO_2/MSU-F-C-3. During heat-treatment under H_2/N_2 (4 wt %) condition, PMA was decomposed to nano-sized molybdenum oxides and the particles were well-dispersed inside the small- and large-pores of MSU-F-C.

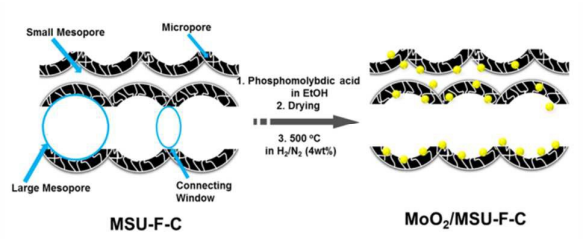

Scheme 1. Schematic illustration of the synthesis of MoO_2-mesocellular carbon foam composite (MoO_2/MSU-F-C).

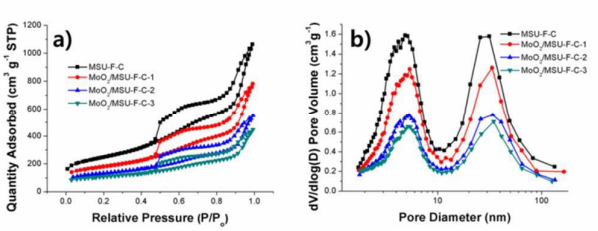

Fig. 1 a) Nitrogen physisorption isotherms and b) BJH pore size distribution graphs of MSU-F-C and MoO_2/MSU-F-C samples.

Table 1. Specific surface area and total pore volume of MSU-F-C and MoO_2/MSU-F-C samples.

	MSU-F-C	MoO_2/MSU-F-C-1	MoO_2/MSU-F-C-2	MoO_2/MSU-F-C-3
specific surface area [m^2 g^{-1}]	880	641	469	384
total pore volume [cm^3 g^{-1}]a	1.64	1.21	0.85	0.69

[a]Measured at P/P_0 = 0.99

Nitrogen physisorption was used to analyze the structural characterizations of the samples (see Fig. 1). Isotherms of the nitrogen physisorption show two distinct capillary condensations at ~0.6 and ~0.9 P/P_o (Fig. 1a). The result indicates that two different sized mesopores are uniformly produced inside the carbons. Brunauer-Emmett-Teller (BET) surface area and pore volume of the MSU-F-C were 880 m^2 g^{-1} and 1.64 cm^3 g^{-1}, respectively. After impregnation of MoO_2 catalyst, the surface area and pore volume decreased with increase in catalyst loading. The values of all the catalysts are

summarized in Table 1. According to Barrett-Joyner-Halenda (BJH) pore size distribution (PSD) calculated from adsorption branches of the isotherms, MSU-F-C took on bimodal pores in the average pore sizes of 5 and 30 nm (Fig. 1b). The PSD peak intensities of both small- and large-pores decreased as catalyst loading increased. This may be attributed to formation of the small nanoparticles that consist of a few nanometer size. SEM images displayed in Fig. S1 also support that there is neither separated particles outside the MSU-F-C nor noticeable MoO_2 particles inside the pores.

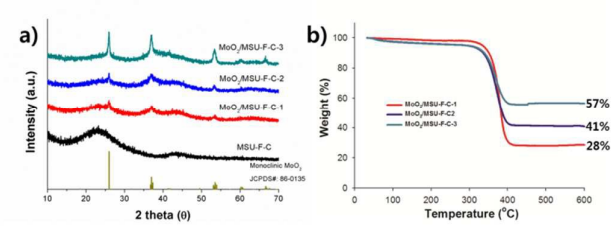

Fig. 2 a) X-ray diffraction patterns of MSU-F-C and MoO_2/MSU-F-C samples and b) thermogravimetric (TG) curves for MoO_2/MSU-F-C samples (heating rate: 2 $^{o}C\ min^{-1}$).

The crystal structures of the samples were investigated by X-ray diffraction (XRD) and the result is represented in Fig. 2a. The XRD pattern of MSU-F-C shows broad two peaks at 23.1 and 43.7°, which corresponds to (002) and (101) diffractions of typical amorphous carbons, while in the MoO_2/MSU-F-C cases, all peaks coincide with those of monoclinic MoO_2 (JCPDS #: 86-0135). The peaks of MoO_2/MSU-F-C-1 and MoO_2/MSU-F-C-2 appeared unclear. The data indicate that ultrafine MoO_2 nanoparticles are well dispersed on the carbon surface or inside the carbon walls.[32] In contrast, MoO_2/MSU-F-C-3 with a high Mo contents shows clear XRD pattern for monoclinic MoO_2, indicating that large sized and exposed MoO_2 nanocrystals were formed, which will be discussed at TEM analysis.

The ratio of metal oxide to carbon was estimated by using thermogravimetric analysis (TGA) under air (Fig. 2b). The weights of MoO_2/MSU-F-C samples were all reduced at 350~400 °C, meaning that amorphous carbons included in composite materials are oxidized. Residual weights of the MoO_2/MSU-F-C-1, -2 and -3 are 28, 41, and 57%, respectively. Theoretical weight increase that occurs during oxidation of MoO_2 to MoO_3 is 12.5%. Based on the theoretical value, the MoO_2 contents in MoO_2/MSU-F-C-1, -2, and -3 were calculated to be 26, 38, and 54 wt%, respectively.

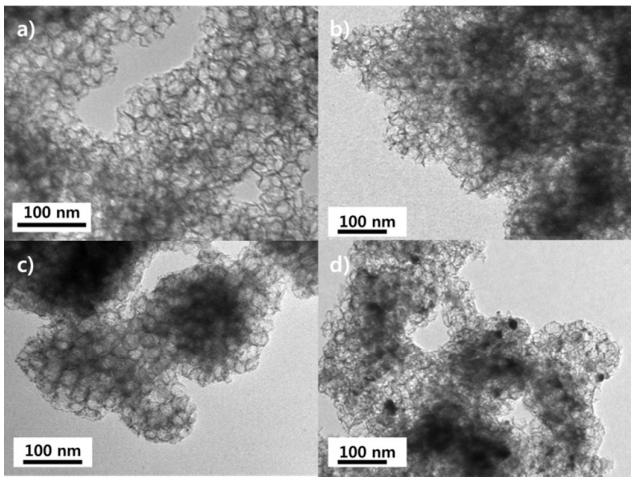

Fig. 3 TEM images of a) MSU-F-C, b) MoO_2/MSU-F-C-1, c) MoO_2/MSU-F-C-2, and d) MoO_2/MSU-F-C-3 samples.

Transmission electron microscopy (TEM) was used to investigate surface morphology of the MoO_2/MSU-F-C catalysts and the TEM images were compared with XRD result. According to the TEM images (Fig. 3a), MSU-F-C shows a typical mesocellular structure containing large-pores (~30 nm), while MoO_2/MSU-F-C-1 and -2 indicate identical porous structures (Figs. 3b and 3c) even after MoO_2 loading, indicating that the MoO_2/MSU-F-C-based structures are advantageous for electrolyte penetration inside the carbon. The MoO_2/MSU-F-C samples also contain well-dispersed and small-sized MoO_2 particles inside the pores (magnified images were displayed in Fig. S2). It may affect vanadium redox reactions in a positive way. In contrast, in MoO_2/MSU-F-C-3 sample, large-sized or agglomerated nanoparticles (< 20 nm) may be formed inside the main pores of MSU-F-C (Fig. 3d).

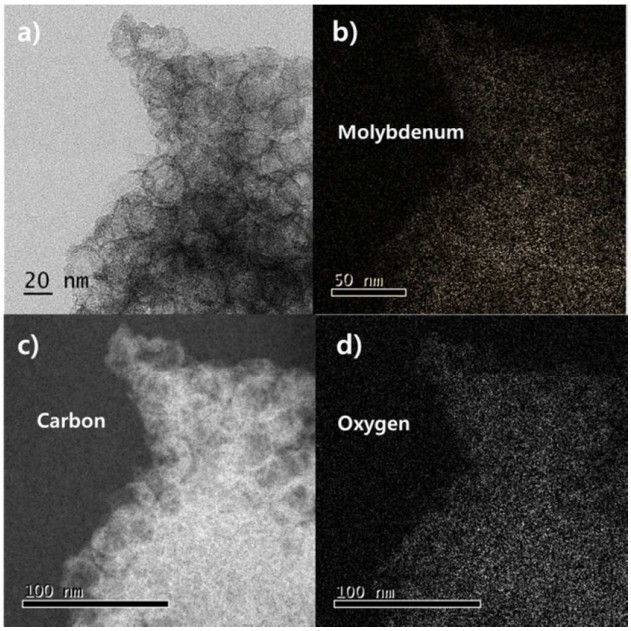

Fig. 4 a) TEM image of MoO_2/MSU-F-C-2 and corresponding EELS images of b) molybdenum, c) carbon, and d) oxygen.

To evaluate whether small sized MoO_2 nanoparticles are embedded well in the pores of MSU-F-C, electron energy loss spectroscopy (EELS) measurements of MoO_2/MSU-F-C-2 of the three samples are performed (Fig. 4). Although noticeable MoO_2 nanoparticles were not observed in TEM images of Fig. 4a, the signals of Mo and O elements were detected around the porous carbon matrix by the EELS. The high resolution TEM images in Fig. S3 also support the XRD, TEM, and EELS data; no noticeable nanocrystals were found in pores or carbon matrix in the MSU-F-C-1 sample, while nanocrystals with a large particle size (~20 nm) were formed in mesopores in MSU-F-C-3 sample. With these results, it was confirmed that small sized MoO_2 nanoparticles were well embedded in the pores of MSU-F-C for MoO_2/MSU-F-C-1 and -2 samples. In the same manner, it is expected that in MoO_2/MSU-F-C-3 sample, relatively larger sized MoO_2 nanoparticles are formed and partly agglomerated inside the main pores of MSU-F-C, expecting that the MoO_2 nanoparticles don't play a key role in catalyzing the vanadium redox reactions.

To investigate the surface structure of catalysts in detail, X-ray photoelectron spectroscopy (XPS) measurements were conducted and peaks of the C 1s and Mo 3d and their deconvolution results were represented in Fig. 5. In the MSU-F-C, C 1s peak corresponds to the typical amorphous carbon structures like C-C and C=C bonds (C1), alcohol or ether (C2), carbonyl (C3), carboxylic acid or ester (C4), and carbonate (C5).[33] After MoO_2 loading, the MoO_2/MSU-F-C-2 sample shows similar carbon C 1s peak (Fig. 5b), proving that the surface functionalities of MSU-F-C are preserved under reductive gas condition. These functional groups of mesoporous carbon can serve as catalytic sites for VO^{2+}/VO_2^+ redox reactions.[5] On the other hand, the three peaks of Mo 3d observed in Fig. 5c represent that the oxidation states of Mo vary in MoO_2/MSU-F-C-2 sample. Although the crystal structure was expected to be monoclinic MoO_2 in the XRD measurement, the deconvolution data show that the major oxidation state of the MoO_2 surface is Mo^{6+}, while Mo^{4+} and Mo^{5+} were the next major oxidation states. The multiple oxidation states observed in reduced MoO_2 surface were compatible with those observed in previous study.[34]

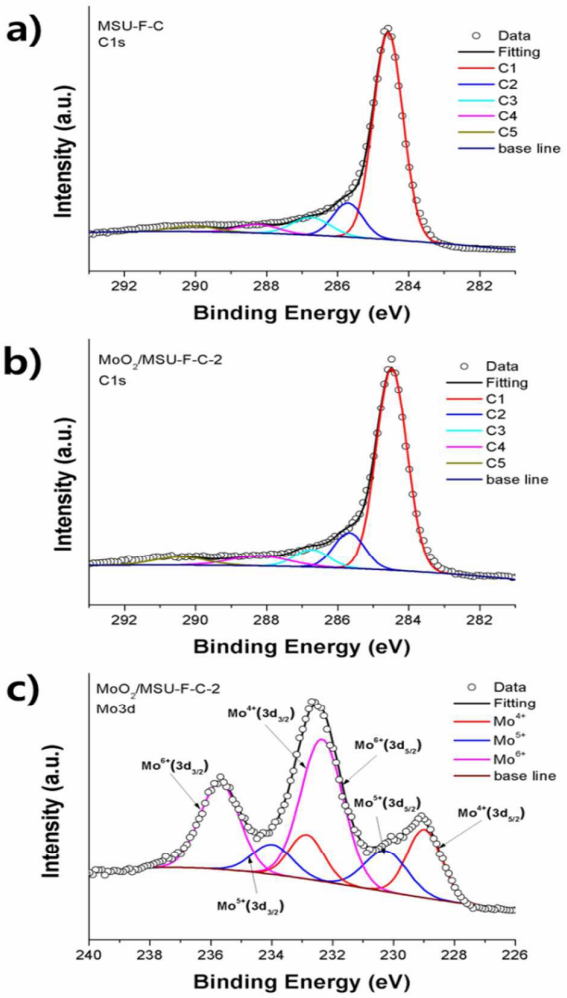

Fig. 5 XPS spectra of a) C1s in MSU-F-C, b) C1s and c) Mo3d in MoO2/MSU-F-C-2.

Although the surface oxidation states of Mo can be produced from Mo to Mo^{6+} depending on calcination conditions, Mo^{4+}~ Mo^{6+} formed mainly in our experiments were due to absorption of oxygen and hydroxyl groups into MoO_2.[31] Moreover, the unsaturated sites such as oxygen vacancy and hydroxyl group created by calcination of MoO_2 take on hydrophilic properties, resulting in improved absorption-ability of the vanadium ions for activating vanadium redox reaction.[34,35] The fact was quantified by measurements of water contact angle. As shown in Fig. S4 a, water contact angle of MoO_2/MSU-F-C (112°) was lower than that of MSU-F-C (139°). It indicates that MoO_2 and mesoporous carbon composite induces better wettability than that of pristine MSU-F-C.This result is also supported by previous studies. According to Jo et al.[36] and Zhou et al.[37], the reduced form of tungsten- or molybdenum-oxides are stable during electrochemical reactions and the multiple oxidation states of transition metal could act as additional catalytic sites due to the increased electron/ion conductivities.

3.2 Optimization of MoO2/MSU-F-C structure

The three types of MoO_2/MSU-F-C; MoO_2/MSU-F-C-1, -2 and -3 were prepared to determine optimal amount of MoO_2 embedded on MSU-F-C. For doing that, their CV curves were evaluated and represented in Fig. 6a. According to Fig. 6a, oxidation and reduction peak currents (I_{pc} and I_{pa}) of MoO_2/MSU-F-C-2 was far better than those of other two catalysts, demonstrating its catalytic activity for activation of the VO^{2+}/VO_2^+ redox reaction was the best. On the other hand, the values of other factors like ratio of reduction to oxidation peak current (I_{pc}/I_{pa}) and difference in reduction and oxidation peak potentials (ΔE_p) were similar in all the samples. This result is well agreed with TEM and EELS data showing (i) insufficient amount of MoO_2 that is embedded on the surface of MSU-F-C (MoO_2/MSU-F-C-1) and (ii) agglomeration of MoO_2 inside MSU-F-C pore (MoO_2/MSU-F-C-3). With compatibility in the structural and electrochemical characterizations, we considered MoO_2/MSU-F-C-2 for the subsequent processes.

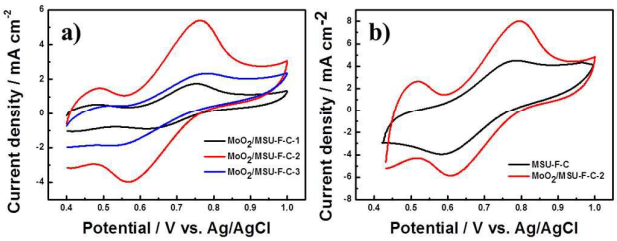

Fig. 6 CV curves of a) MoO_2/MSU-F-C-1, MoO_2/MSU-F-C-2, and MoO_2/MSU-F-C-3 catalysts and b) MoO_2/MSU-F-C-2 and MSU-F-C catalysts measured under electrolyte of 0.1 M $VOSO_4$ + 0.1 M H_2SO_4. Potential scan rate for a) and b) data was 70 and 100 mV $^{s-1}$, respectively, and potential scan range of CVs was from 0.4 to 1.0 V vs. Ag/AgCl.

3.3. Effects of MoO_2/MSU-F-C catalyst on catalytic activity of redox reaction of VO^{2+}/VO_2^+

To investigate MoO_2 effect on activity and reversibility of VO^{2+}/VO_2^+ reaction, CV curves of MSU-F-C and MoO_2/MSU-F-C-2 catalysts were measured and electrochemical properties like (i) I_{pc} and I_{pa}, (ii) I_{pc}/I_{pa} and (iii) ΔE_p of the two catalysts were compared (see Fig. 6b). According to the Fig. 6b, peak currents and ΔE_p of MoO2/MSU-F-C-2 (I_{pc} and I_{pa} are 10.0 and 8.1 mA cm^{-2}, while ΔE_p was 256 mV) were better than those of MSU-F-C (I_{pc} and I_{pa} are 6.8 and 6.2 mA cm^{-2}, while ΔE_p was 265 mV), implying that the MoO_2/MSU-F-C-2 facilitated catalytic activity and reversibility for VO^{2+}/VO_2^+ redox reaction.

Following the evaluation of MoO_2 effect on VO^{2+}/VO_2^+ redox reaction (positive electrode), MoO_2 effect on V^{2+}/V^{3+} redox reaction (negative electrode) was also estimated to inspect whether the MoO_2/MSU-F-C-2 catalyst affects (i) the V^{2+}/V^{3+} redox reaction or (ii) undesirable hydrogen evolution reaction because the two reactions take place at the similar potential range. For doing that, CV curves of MSU-F-C and MoO_2/MSU-F-C-2 catalysts were measured in the corresponding potential range (Fig. S5).

According to the Fig. S5, MoO_2/MSU-F-C-2 did not induce any redox peak at -0.4 ~ -0.6 V vs. Ag/AgCl that was potential range of both V^{2+}/V^{3+} and hydrogen evolution reactions. On the other hand, MSU-F-C showed V^{2+}/V^{3+} reaction peaks at the potential range, meaning that MoO_2 embedded on MSU-F-C did not lead to V^{2+}/V^{3+} reaction, while MSU-F-C itself could help to promote V^{2+}/V^{3+} reaction. With the CV curves of Fig. S5, it could be explained that MoO_2/MSU-F-C-2 was an effective catalyst for only VO^{2+}/VO_2^+ redox reaction, confirming that the MoO_2/MSU-F-C-2 could be considered catalyst for the positive electrode of VRFB.

Electron transfer rate constant, k_s, of MoO_2/MSU-F-C-2 and MSU-F-C catalysts were measured because the k_s is a key index (i) to quantify how fast electrons are transferred during the VO^{2+}/VO_2^+ redox reaction and (ii) to check out whether MoO_2/MSU-F-C-2 induces faster electron transfer rate than MSU-F-C. To do that, CV curves of the two catalysts were measured under different scan rates using Laviron's formula.[4,5] With that, the k_ss of MoO_2/MSU-F-C-2 and MSU-F-C catalysts were calculated as 0.33 and 0.11 s^{-1}, respectively, exhibiting k_s of the MoO_2/MSU-F-C-2 was three times higher than that of MSU-F-C. This result is compatible with catalytic activity and reversibility tendency shown in Fig. S6.

We also investigated the effect of potential scan rate on catalytic activity of the MoO_2/MSU-F-C-2 layer and the result is represented in Fig. S7. In the measurements, the redox peak currents linearly increased as the scan rate increased, demonstrating that MoO_2/MSU-F-C-2 is controlled by a surface reaction confined process.

3.4 Effect of MoO2/MSU-F-C catalyst on VRFB performance

To inspect whether catalytic activity and reversibility of VO^{2+}/VO_2^+ redox reaction have any influence on VRFB performance, charge-discharge curves of (i) VRFB single cells including two catalysts (MoO_2/MSU-F-C-2 and MSU-F-C) and (ii) no catalyst-adopted VRFB single cell were measured. Since the catalysts mostly affected VO^{2+}/VO_2^+ redox reaction, they were only embedded at positive electrode. The different VRFBs are denoted as pristine graphite felt (Pristine-VRFB), MSU-F-C-deposited graphite felt (MSU-F-C-VRFB) and MoO_2/MSU-F-C-2-deposited graphite felt (MoO_2/MSU-F-C-2-VRFB).

According to the result (Fig. S8), MoO_2/MSU-F-C-2-VRFB indicated higher discharging and lower charging potentials than MSU-F-C-VRFB and Pristine-VRFB. It means that overall overpotential of the MoO_2/MSU-F-C catalyst is low. A vertical potential drop was also estimated to measure internal resistance of the corresponding VRFB.[33] As same to overpotential trend, MoO_2/MSU-F-C-2-VRFB exhibited lowest potential drop, followed by lowest internal resistance. With these data, it is anticipated that MoO_2/MSU-F-C-2-VRFB will induce higher voltage efficiency (VE) than other VRFBs because the VE relies on overpotential and internal resistance. They also affect reactivity (catalytic activity and reversibility) of VO^{2+}/VO_2^+ redox reaction. Taken together, it is obvious that MoO_2/MSU-F-C-2-VRFB showing (i) excellent reactivity of VO^{2+}/VO_2^+ redox reaction and (ii) low overpotential and potential drop improves VRFB performance, while MoO_2 plays a dominant role in extracting such a good VRFB performance.

Fig. S9 shows specific discharge capacities of the three VRFBs that were measured after every five cycles. According to the Fig. S9, discharge capacity of MoO_2/MSU-F-C-2-VRFB was the highest compared to that of MSU-F-C-VRFB and Pristine-VRFB, while its capacity loss rate was better than MSU-F-C-VRFB and compatible with Pristine-VRFB. It implies that the discharge capacity and capacity loss of MoO_2/MSU-F-C-2-VRFB are viable.

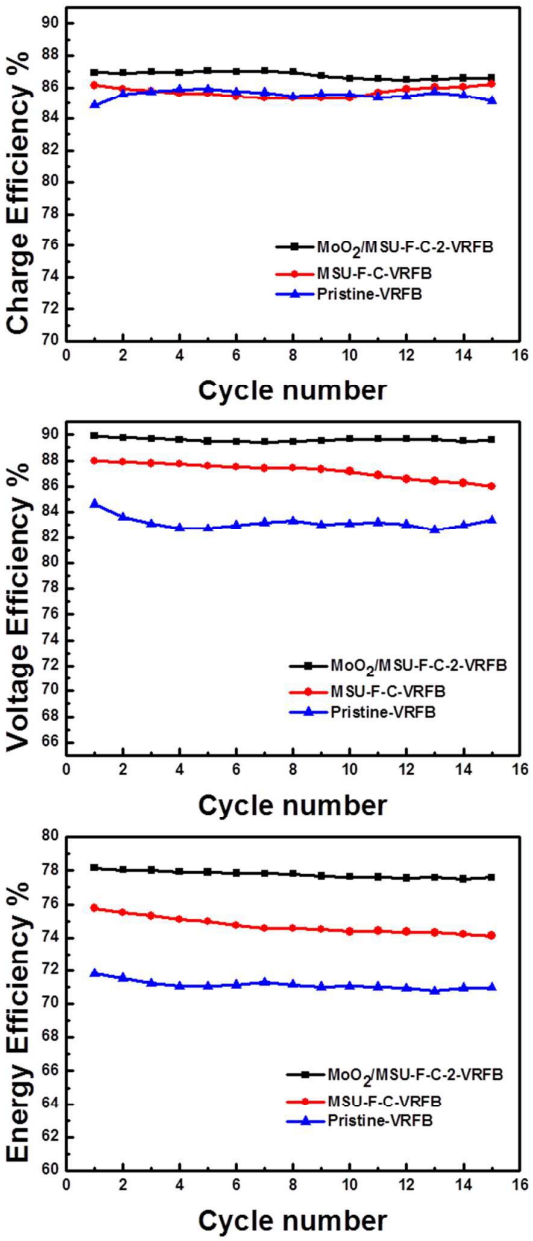

Fig. 7 Charge efficiency, power efficiency and energy efficiency of VRFB single cells consisting of MoO_2/MSU-F-C-2, MSU-F-C catalysts, and graphite felt as positive electrode at current density of 40 mA cm^{-2}.

To evaluate performance of the three VRFBs, the three efficiencies (charge efficiency (CE), VE and EE) were measured and the result is represented in Fig. 7. According to Fig. 7, MoO_2/MSU-F-C-2-VRFB demonstrated higher VE and EE than other VRFBs (MSU-F-C-VRFB and Pristine-VRFB), while difference in CE was not large enough. Difference in VE is mainly due to difference in potential losses of overpotential and internal resistance as explained previously. Since the charge-discharge behavior of MoO_2/MSU-F-C-2-VRFB had low potential loss, difference in charge and discharge potentials of the VRFBs was also low, resulting in an increase in VE that was a ratio of charge and discharge potentials.[38] Unlike the VE, CE is determined by difference in amount of charges transferred during the charge and discharge step that was crossovered via Nafion 212 membrane. This CE result means that the difference in amount of charges permeated via the membrane is not large in all three VRFBs. With this explanation, it is expected that EE was more affected by VE.

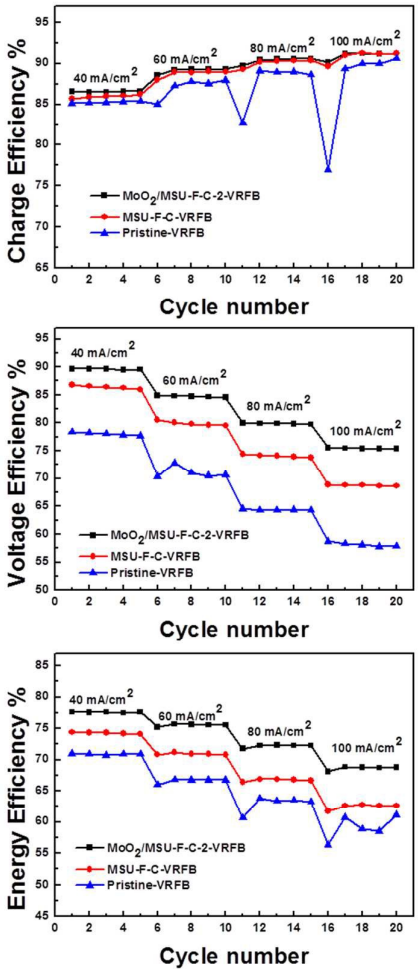

Fig. 8 Charge efficiency, power efficiency and energy efficiency of VRFB single cells consisting of MoO_2/MSU-F-C-2, MSU-F-C catalysts, and graphite felt as positive electrode at different current densities of 40 ~ 100 mA cm^{-2}.

To further estimate CE and VE effects on EE of VRFBs, the efficiencies of VRFBs were again measured with increase in current density and the result is represented in Fig. 8. For the tests, applied current densities were ranged from 40 to 100 mA cm^{-2} by increment of 20 mA cm^{-2}. With the efficiency data, there are two things to notify. First, CE increased with increase in current density. It means that with increase in current density, (i) amount of charge produced increases and (ii) amount of charge transferred during the charge and discharge step are getting equalized, resulting in increase in CE. Furthermore, in high current densities (80 and 100 mA cm^{-2}), CE of MSU-F-C-VRFB and Pristine-VRFB was unstable, while that of MoO_2/MSU-F-C-2-VRFB remained stable. Unlike stability, increasing rate of CE in all the three VRFBs with increase in current density was similar together. Based on the result, it can be induced that MoO_2 belonging to MoO_2/MSU-F-C-2 catalyst leads to the superior CE stability.

Second, VE decreased with increase in current density. It indicates that with increase in current density, overpotential and internal resistance increase due to ohm's law, reducing VE. Like CE, in high current densities, VE of MSU-F-C-VRFB and Pristine-VRFB was unstable, while that of MoO_2/MSU-F-C-2-VRFB remained stable. With the increase in current density, VE loss rate in MoO_2/MSU-F-C-2-VRFB is lower than that in other VRFBs. This result indicates that the MoO_2 results in the excellent VE stability and low VE loss rate with increase in current density. Regarding EE, the EE showed similar trend to VE, confirming that VE played more dominant role than CE in determining EE of VRFBs.

3.5. Role of MoO_2 and MSU-F-C on VRFB performance

Based on the half-cell and single cell data, it can be explained that MoO_2/MSU-F-C-2 catalyst results in superior catalytic activity and reversibility for activation of the VO^{2+}/VO_2^+ redox reaction, while MoO_2/MSU-F-C-2-VRFB leads to excellent VE and EE, more discharge capacity and less capacity loss even in high current density range. It was induced that employment of MoO_2 as the catalyst made such differences in the half-cell and single cell data.

With the adoption of MoO_2, there are three advantages to notify. First, interconnected structure between MoO_2 and MSU-F-C is supposed to promote fast ionic and electron transfers as well as reduction in overpotential and internal resistance. According to Chernova et al.[39] MoO_2 can be intercalated by metal cations like VO^{2+} and VO_2^+ and the intercalated structure makes a good conductor role. This phenomenon is also called as "mixed conductor". Indeed, the structure facilitates (i) superior ionic and electron conductivity and (ii) low charge resistance. Due to the reason, it is likely that MoO_2/MSU-F-C-2 structure shows excellent electron conductivity as well as low resistances. It was confirmed by high k_s, VE and EE values. This result was also well agreed with previous published materials.[40]

Second, MoO_2 induced more hydrophilic functional ions like oxygen vacancy and hydroxyl group at the catalyst surface as observed in XPS data (Fig. 5). Following that, such hydrophilic groups played a role in reducing activation barrier for VO^{2+}/VO_2^+ redox reaction, producing faster charge transfer.[18,41]

Third, mesoporous structure including MoO_2 facilitates diffusion of liquid electrolyte into carbon felt electrode using the capillary action. It means that MoO_2/MSU-F-C-2 structure induces fast conductive ion transport channels for conductive ions such as VO^{2+} and VO_2^+.[42-44]

Conclusions

A new MoO_2/MSU-F-C catalyst was used for VRFB to improve slow reaction of VO^{2+}/VO_2^+ redox couple. A few nanometer-sized MoO_2 particles are loaded on the surface of MSU-F-C. The 3-D structured large pores (~30 nm) facilitate the electrolyte wetting and promote the redox reaction in VRFB. Due to the additional catalytic effect of the hydrophilic MoO_2, the MoO_2/MSU-F-C-2 composite exhibited improved catalyst properties. When activity and reversibility of the MoO_2/MSU-F-C catalyst were evaluated, the catalyst led to high peak currents (5.4 mA cm^{-2} and 4.0 mA cm^{-2}), small peak potential difference (256 mV) and high electron transfer rate constant (0.33 s^{-1}), turning out that the catalyst catalyzed VO^{2+}/VO_2^+ redox reaction favorably.

When it came to the multiple charge/discharge cycle tests, MoO_2/MSU-F-C-VRFB produced high VE and EE (VE: 89 % and EE: 76 %), high specific capacity, low capacity loss rate and no significant changes in efficiencies even in high current density of 100 mA cm^{-2}.

Such superior half-cell and single cell results gained by using MoO_2/MSU-F-C catalyst are ascribed to the following three reasons. First, intercalation of MoO_2 occurred by metal cations like VO^{2+} and VO_2^+, second, large portion of hydrophilic functional groups doped on the surface of MoO_2/MSU-F-C and third, mesoporous structure including MoO_2 that enabled facile diffusion of liquid electrolyte into carbon felt electrode. All of the desirable characteristics obtained by employment of MoO_2 or MoO_2/MSU-F-C promote VO^{2+}/VO_2^+ redox reaction by making carbon felt electrode more conductive/diffusional and easier to react. Eventually, it turned out that adoption of MoO_2/MSU-F-C resulted in improvement in VRFB performance by promoting the slow VO^{2+}/VO_2^+ redox reaction.

Acknowledgements

This research was supported by Basic Science Research Program through the National Research Foundation of Korea (NRF) funded by the Ministry of Education (NRF-2013R1A1A2006494).

Notes and references

1 Y. Shao, X. Wang, M. Engelhard, C. Wang, S. Dai, J. Liu, Z. Yang, and Y. Lin, *J. Power Sources*, 2010, **195**, 4375-4379.
2 A.Z. Weber, M.M. Mench, J.P. Meyers, P.N. Ross, J.T. Gostick, and Q.H. Liu, *J. Appl. Electrochem*., 2011, **41**, 1137-1364.
3 Z. González, C. Botas, P. Álvarez, S. Roldán, C. Blanco, R. Santamaría, M. Granda, and R. Menéndez, *Carbon*, 2012, **50**, 828-834.
4 S. Jeong, S. Kim, and Y. Kwon, *Electrochim. Acta*, 2013, **114**, 439-447.
5 S. Jeong, S. An, J. Jeong, J. Lee, and Y. Kwon, *J. Power Sources*, 2015, **278**, 245-254.

6 S. Jeong, L. Kim, Y. Kwon, and S. Kim, *Korean J. Chem. Eng.*, 2014, **23**, 2081-2087.
7 W. Li, J. Liu, and C. Yan, *Carbon*, 2013, **55**, 313-320.
8 D. Chen, M.A. Hickner, E. Agar, and E.C. Kumbur, *ACS Appl. Mater. Interfaces*, 2013, **5**, 7559−7566.
9 Z. Li, W. Dai, L. Yu, L. Liu, J. Xi, X. Qiu, and L. Chen, *ACS Appl. Mater. Interfaces*, 2014, **6**, 18885-18893.
10 G. Oriji, Y. Katayama, and T. Miura, *J. Power Sources*, 2005, **139**, 321-324.
11 C. Yao, H. Zhang, T. Liu, X. Li, and Z. Liu, *J. Power Sources*, 2012, **218**, 455-461.
12 W. Zhang, J. Xi, Z. Li, H. Zhou, L. Liu, Z. Wu, and X. Qiu, *Electrochim. Acta*, 2013, **89**, 429-435.
13 P. Han, H. Wang, Z. Liu, X. Chen, W. Ma, J. Yao, Y. Zhu, and G. Cui, *Carbon*, 2011, **49**, 693-700.
14 S. Zhong, and M. Skyllas-Kazacos, *J. Power Sources*, 1992, **39**, 1-9.
15 M. Gattrell, J. Park, B. MacDougall, J. Apte, S. McCarthy, and C.W. Wu, *J. Electrochem. Soc.*, 2004, **51**, A123-A130.
16 J. Xi, W. Zhang, Z. Li, H. Zhou, L. Liu, Z. Wu, and X. Qiu, *Int. J. Electrochem. Sci.*, 2013, **8**, 4700-4711.
17 T.M. Tseng, R.H. Huang, C.Y. Huang, K.L. Hsueh, and F.S. Shieu, *J. Electrochem. Soc.*, 2013, **160(4)**, A690-A696.
18 W.H. Wang, and X.D. Wang, *Electrochim. Acta*, 2007, **52**, 6755-6762.
19 H.M. Tsai, S.L. Yang, C.C.M. Ma, and X. Xie, *Electrochim. Acta*, 2012, **77**, 232-236.
20 K.J. Kim, M.S. Park, J.H. Kim, U. Hwang, N.J. Lee, G. Jeong, and Y.J. Kim, *Chem. Commun.*, 2012, **48**, 5455-5457.
21 B. Li, M. Gu, Z. Nie, X. Wei, C. Wang, V. Sprenkle, and W. Wang, *Nano Lett.*, 2014, **14**, 158-165.
22 B. Sun, and M. Skyllas-Kazakos, Electrochim. Acta, 1992, 52, 1253-1260.
23 Z. Wang, J.S. Chen, T. Zhu, S. Madhavi, and X.W. Lou, *Chem. Commun.*, 2010, **46**, 6906-6908.
24 L. Yang, L. Liu, Y. Zhu, X. Wang, and Y. Wu, *J. Mater. Chem.*, 2012, **22**, 13148-13152.
25 X. Zhang, X. Song, S. Gao, Y. Xu, X. Cheng, H. Zhao, and L. Huo, *J. Mater. Chem. A*, 2013, **1**, 6858-6864.
26 S.S. Kim, T.R. Pauly, and T.J. Pinnavaia, *Chem. Commun.*, 2000, **17**, 1661-1662.
27 J. Lee, K. Sohn, and T. Hyeon, *Chem. Commun.*, 2012, **22**, 2674-2675.
28 K. Hyun, J.H. Lee, C.W. Yoon, and Y. Kwon, *Int. J. Electrochem. Sci.*, 2013, **8**, 11752-11767.
29 K. Hyun, J.H. Lee, C.W. Yoon, Y.H. Cho, L.H. Kim, and Y. Kwon, *Synth. Met.*, 2014, **190**, 48-55.
30 E. Kang, Y.S. Jung, A.S. Cavanagh, G.H. Kim, S.M. George, A.C. Dillon, J.K. Kim, and J. Lee, *Adv. Funct. Mater.*, 2011, **21**, 2430-2438.
31 C. Jo, S. An, Y. Kim, J. Shim, S. Yoon, and J. Lee, *Phys. Chem. Chem. Phys.*, 2012, **14**, 5695-7504.
32 K. H. Seng, G. D. Du, L. Li, Z. X. Chen, H. K. Liu, Z. P. Guo, *J. Mater. Chem.,* 2012, **22**, 16072-16077.
33 S.D. Gardner, C.S.K. Singamsetty, G.L. Booth, G.R. He, and C.U. Pittman, *Carbon*, 1995, **33**, 587-595.
34 J. Baltrusaitis, B. Mendoza-Sanchez, V. Fernandez, R. Veenstra, N. Dukstiene, A. Roberts, and N. Fairley, *Appl. Surf. Sci.*, 2015, **326**, 151-161.
35 J.G. Choi, and L.T. Thompson, *Appl. Surf. Sci.*, 1996, **93**, 143-149.
36 C. Jo, J. Hwang, H. Song, A.H. Dao, Y.T. Kim, S.H. Lee, S.W. Hong, S. Yoon, and J. Lee, *Adv. Funct. Mater*, 2013, **23**, 3747-3754.
37 Y. Zhou, C.W. Lee, and S. Yoon, *Electrochem. Solid-State Lett.*, 2011, **14**, A157-A160.
38 D. Chen, M.A. Hickner, E. Agar, and E.C. Kumbur, *J. Membr. Sci.*, 2013, **437**, 108-113.
39 N.A. Chernova, M. Roppolo, A.C. Dillon, and M.S. Whittingham, *J. Mater. Chem.*, 2009, **19**, 2526-2552.
40 L. Zhou, H.B. Wu, Z. Wang, and X.W. Lou, *ACS Appl. Mater. Interfaces*, 2011, **3**, 4853-4857.
41 J.S. Lee, T. Lee, H.K. Song, J. Cho, and B.S. Kim, *Energy Environ. Sci.*, 2011, **4**, 4148-4154.
42 Y. Shi, B. Guo, S.A. Corr, Q. Shi, Y.S. Hu, K.R. Heier, L. Chen, R. Seshadri, and G.D. Stucky, *Nano Lett.*, 2009, **9(12)**, 4215-4220.
43 L.J. Fu, T. Zhang, Q. Cao, H.P. Zhang, and Y.P. Wu, *Electrochem. Commun.*, 2007, **9**, 2140-2144.
44 Y. Ye, C. Jo, I. Jeong, and J. Lee, *Nanoscale*, 2013, **5**, 4584-4605.

Graphical abstract